

## Aerosol optical properties from the Atmospheric Radiation Measurement Mobile Facility at Shouxian, China

Xuehua Fan,<sup>1</sup> Hongbin Chen,<sup>1</sup> Xiangao Xia,<sup>1</sup> Zhanqing Li,<sup>2</sup> and Maureen Cribb<sup>2</sup>

Received 20 June 2010; revised 25 September 2010; accepted 5 October 2010; published 17 December 2010.

[1] The Atmospheric Radiation Measurement program's Mobile Facility was deployed at Shouxian, China (32.56°N, 116.78°E, elevation 22.7 m), from May to December 2008. Aerosol optical properties derived from the Aerosol Observation System (AOS) measurements are analyzed. The median value of the light scattering coefficient ( $\sigma_{sp}$ ) at 550 nm is 302.8 Mm<sup>-1</sup>. The lowest value of  $\sigma_{sp}$  appeared in the summer and was mainly due to strong wet deposition and upward transport. Averaged over the measurement period from May to July (arithmetic mean  $\pm$  standard deviation), the aerosol light absorption coefficient,  $\sigma_{ap}$ , is 29.4  $\pm$  31.1 Mm<sup>-1</sup> (550 nm) which is lower than most measurements made in urban areas in China but higher than those observed in background sites such as Shangdianzi, a suburb of Beijing. The mean single scattering albedo ( $\omega_o$ ) is 0.92, which is greater than values found in the Pearl River Delta, the Yangtze Delta, and northern China, indicating less absorbing aerosols at the Shouxian site. The mean values and standard deviations of the Ångström exponent ( $\alpha$ , 700–550 nm), the submicron scattering ratio ( $R_{sp}$ ), and the hemispheric backscattering ratio ( $b$ ) at 550 nm are 1.19  $\pm$  0.23, 0.47  $\pm$  0.15, and 0.101  $\pm$  0.017, respectively. These values are lower than those observed at continental sites in the United States, implying the relatively large contributions of coarse mode particles at Shouxian. A distinct diurnal variation of aerosol optical properties is observed. Absorption coefficients are highest in the early morning and minimum values appear at noon. The  $\omega_o$  shows nearly the same cycle as the absorption coefficient but with the maximum and minimum reversed. Impacts of local agricultural residue burning and long-range transport of dust on aerosol loading and properties are presented using Moderate Resolution Imaging Spectrometer (MODIS) fire spot data, MODIS level-2 aerosol optical depth data and micropulse lidar data together with AOS data.

**Citation:** Fan, X., H. Chen, X. Xia, Z. Li, and M. Cribb (2010), Aerosol optical properties from the Atmospheric Radiation Measurement Mobile Facility at Shouxian, China, *J. Geophys. Res.*, 115, D00K33, doi:10.1029/2010JD014650.

### 1. Introduction

[2] Aerosol radiative forcing is one of the greatest sources of uncertainty in climate modeling. Aerosols directly impact the energy budget of the atmosphere. On the other hand, aerosols, as cloud condensation nuclei (CCN), can modulate cloud microphysical processes, which could indirectly impact cloud radiative properties and climate. The rapid growth of industrialization and urbanization in China has led to a significant increase in aerosol particles (such as both soot and sulfate) in China. Aerosol optical depth is estimated to have increased from 0.38 in 1960 to 0.47 in 1990 [Luo *et al.*, 2001]. Aerosol composition and sources in eastern China are

very complex, including not only anthropogenic aerosols from human activities, but also natural aerosols from remote dust storms transported to the region [Jin and Shepherd, 2008]. High aerosol loading is observed in eastern China with a mean aerosol optical depth (AOD) of 0.5 [Z. Li *et al.*, 2007a]. Analyses of Moderate Resolution Imaging Spectrometer (MODIS) aerosol products showed that aerosols in the eastern part of China are closely related to human activities [Li *et al.*, 2003]. Preliminary analyses of multiple satellite data sets over eastern China indicate complex and unique aerosol direct and indirect effects, which might impact cloud reflectivity and precipitation processes [Yu *et al.*, 2001; Li *et al.*, 2003; Zhao *et al.*, 2006; Jin and Shepherd, 2008; Bao *et al.*, 2009]. The increase in aerosol loading likely partly accounts for the notable decrease in sunshine duration and surface irradiance [Che *et al.*, 2005; Liang and Xia, 2005; Qian *et al.*, 2006]. Regional changes in temperature and precipitation patterns since the mid-1970s in China may be related to heavy aerosol loading and strong absorption by aerosols [Li and Zhou, 1995; Xu, 2001; C. Li *et al.*, 2007].

<sup>1</sup>Key Laboratory of Middle Atmosphere and Global Environment Observation, Institute of Atmospheric Physics, Chinese Academy of Sciences, Beijing, China.

<sup>2</sup>Department of Atmospheric and Oceanic Sciences, University of Maryland, College Park, Maryland, USA.

**Table 1.** AOS Instruments and Atmospheric Measurements Made at Shouxian

Instrument	Primary Measurements	Derived Measurements
TSI Model 3563 three-wavelength nephelometer at both low (<40%) and variable (~40–90%) relative humidity	total scattering coefficients ( $\sigma_{sp}$ ); hemispheric backscattering coefficients ( $\sigma_{bsp}$ ) from $D_p < 1 \mu\text{m}$ and $D_p < 10 \mu\text{m}$ particles at 450, 550, and 700 nm	hemispheric backscattering fraction ( $b$ ); Ångström exponent ( $\alpha$ ); submicron scattering fraction ( $R_{sp}$ )
Radiance Research Model PSAP particulate light absorption photometer	light absorption coefficient ( $\sigma_{ap}$ ) from $D_p < 1 \mu\text{m}$ and $D_p < 10 \mu\text{m}$ particles at 565 nm	single scattering albedo ( $\omega_a$ ) at 550 nm

[3] In order to verify satellite observations and gain a deeper understanding of aerosol effects on climate and the environment, in situ measurements and ground-based remote sensing data are urgently needed. A 1 month observation period during November 1999 in Linan, about 46 km west of Hangzhou City, showed that the mean (standard deviation) mass scattering efficiency of dry aerosols and the mass absorption efficiency of elemental carbon were  $4.0 \text{ m}^2 \text{ g}^{-1}$  ( $0.4 \text{ m}^2 \text{ g}^{-1}$ ) and  $8.6 \text{ m}^2 \text{ g}^{-1}$  ( $7.0 \text{ m}^2 \text{ g}^{-1}$ ), respectively [Xu *et al.*, 2002]. Studies on aerosol optical properties and their radiative effects were carried out in both southern and northern China at Taihu surrounded by big cities in the Yangtze delta region [Xia *et al.*, 2007] and at Xianghe between the big cities of Beijing and Tianjin [Z. Li *et al.*, 2007b]. Heavy aerosol loadings and strong aerosol absorption in these region lead to substantial reductions in direct and global shortwave irradiances at the surface, but the instantaneous aerosol direct radiative forcing at the top of the atmosphere is close to zero due to the moderate absorption properties of aerosols at both sites. This finding appears to be ubiquitous in China, as revealed by the values of aerosol radiative forcing derived at 24 stations across China [Li *et al.*, 2010] estimated from a combination of satellite and ground-based observations [Xin *et al.*, 2007]. The spatial and temporal characteristics of AODs and Ångström exponents and their relationship to aerosol chemical compositions were analyzed using data from the CE318 Sun photometer and aerosol sampling instruments at Linan, Shangdianzi, and Longfengshan regional atmospheric background stations in China [Che *et al.*, 2009]. Song and Lu [2006] used Sun photometer data from 2000 to 2002 to obtain the seasonal variation of AOD over Shanghai City. Aerosol optical properties retrieved from simultaneous Sun photometer measurements made at different sites in the Chinese Yangtze Delta Region were studied by Pan *et al.* [2010].

[4] Retrievals of AOD and Ångström exponent were also made in the downtown and suburban areas of Hangzhou City [Chen *et al.*, 2008]. There has been very limited in situ measurement of aerosol optical properties in China which is crucial to understand aerosol properties and their climate and environmental impact.

[5] In order to study aerosol indirect effects in China, the ARM (Atmospheric Radiation Measurement) Mobile Facility (AMF) was deployed in Shouxian, approximately 500 km northwest of Shanghai City from May to December 2008. Simultaneous observations of cloud, aerosol, radiative properties and meteorological factors were made in this key region for the first time, as far as we know.

[6] The objective of this study is to analyze the aerosol properties derived from AMF Aerosol Observing System (AOS) measurements. Section 2 briefly introduces the AOS

instruments and data. Time series and the diurnal variation of aerosol optical properties are presented in section 3. Section 3 also includes the investigation of two extreme pollution episodes using a combination of AOS aerosol properties, micropulse lidar (MPL) data, MODIS satellite data and backward trajectories. The summary is given in section 4. The analysis results presented here would be instrumental to reveal and understand the direct and indirect effects of aerosols in the region.

## 2. Aerosol Observation System and Data at the Shouxian Site

### 2.1. Instruments and Data

[7] The AOS is the primary ARM platform for in situ observation of aerosol properties. The AOS comprises a set of instruments designed primarily for measuring aerosol microphysical and optical properties. Quantities measured by the AOS include total scattering coefficients ( $\sigma_{sp}$ ), hemispheric backscattering coefficients ( $\sigma_{bsp}$ ), and light absorption coefficients ( $\sigma_{ap}$ ). A summary of AOS instruments, measured parameters, and the derived aerosol properties is given in Table 1.

[8] The total light scattering and hemispheric backscattering coefficients of aerosols are measured by a TSI Model 3563 three-wavelength (450, 550, and 700 nm) nephelometer at a relative humidity (RH) below 40% to minimize the effects of changing relative humidity on measurements [Peppler *et al.*, 2000]. Another TSI nephelometer is connected to a humidity scanning system to provide measurements of scattering coefficients as a function of RH. The nephelometers are calibrated weekly using  $\text{CO}_2$  gas. The light absorption coefficient is measured by a Radiance Research Particle/Soot Absorption Photometer (Model PSAP) at 565 nm. A correction scheme was developed [Bond *et al.*, 1999] to derive the light absorption coefficient at 550 nm from PSAP reported absorption values and is given by

$$\sigma_{ap}^{550} = (\sigma_{adj}^{565} - K_1 \sigma_{sp}^{550}) / K_2, \quad (1)$$

where  $\sigma_{ap}^{550}$  is the true atmospheric aerosol light absorption coefficient at 550 nm,  $\sigma_{adj}^{565}$  is the instrument absorption coefficient at 565 nm obtained after flow and spot size corrections are applied;  $\sigma_{sp}^{550}$  is the aerosol scattering coefficient at 550 nm.  $K_1$  and  $K_2$  are the PSAP response to scattering and absorption with empirical values of 0.02 and 1.22, respectively.

[9] The raw sampling interval of all AOS measurements is 1 min. Before light scattering and absorption measurements are made, each aerosol sample passes through an inertial impactor with a 50% cutoff particle diameter at either  $1 \mu\text{m}$  (alternate size) or  $10 \mu\text{m}$  (default size). An automated inlet

switch operating at a 5 min switching frequency is used to direct the air sample to the 1 or 10  $\mu\text{m}$  impactor in order to remove large particles [Peppler *et al.*, 2000]. Hourly averaged data from the ARM archive are used directly in the analysis. Daily averaged data in the paper are derived from this hourly averaged data.

[10] From the measurements mentioned above, it is possible to determine the hemispheric backscatter fraction ( $b$ ), Ångström exponent ( $\alpha$ ), aerosol single scattering albedo (SSA,  $\omega_o$ ), and submicron scattering fraction ( $R_{sp}$ ). These parameters are calculated by using the following formulas:

$$b = \frac{\sigma_{bsp}}{\sigma_{sp}}, \quad (2)$$

$$\alpha = -\frac{\log(\sigma_{sp1}/\sigma_{sp2})}{\log(\lambda_1/\lambda_2)}, \quad (3)$$

$$\omega_o = \frac{\sigma_{sp}}{\sigma_{sp} + \sigma_{ap}}, \quad (4)$$

$$R_{sp} = \frac{\sigma_{sp}(D_p < 1\mu\text{m})}{\sigma_{sp}(D_p < 10\mu\text{m})}, \quad (5)$$

where  $\sigma_{bsp}$  and  $\sigma_{sp}$  in equation (2) are the hemispheric backscatter coefficient and total scattering coefficient, respectively, in units of  $\text{Mm}^{-1}$ ;  $\sigma_{ap}$  in equation (4) is the absorption coefficient with the unit of  $\text{Mm}^{-1}$ ;  $\sigma_{sp}(D_p < 1\mu\text{m})$  and  $\sigma_{sp}(D_p < 10\mu\text{m})$  in equation (5) represent the total scattering coefficients for particle diameter less than 1  $\mu\text{m}$  and less than 10  $\mu\text{m}$ , respectively. Here  $\omega_o$  is referenced to 550 nm, both  $b$  and  $R_{sp}$  are referenced to 450, 550 and 700 nm, and  $\lambda$  in equation (3) refers to wavelength; and subscripts 1 and 2 denote  $\sigma_{sp}$  and  $\lambda$  at different wavelengths. Since  $\sigma_{sp}$  was measured at three wavelengths, three values of  $\alpha$  are computed for each  $\sigma_{sp}$  measurement. The four derived parameters ( $b$ ,  $\alpha$ ,  $\omega_o$  and  $R_{sp}$ ) are dimensionless quantities.

## 2.2. Shouxian Site Description

[11] The AOS system was deployed at Shouxian, China (32.56°N, 116.78°E, elevation 22.7 m) from 8 May to 28 December 2008. Shouxian, in the province of Anhui, is located on the south bank of the Huaihe River, less than 200 km from the Yangtze River and about 500 km northwest of Shanghai City. The annual mean temperature is about 14.8°C; mean temperatures in January and July are about 0.7°C and 27.9°C, respectively. The annual mean precipitation is 906 mm. The population in Shouxian (a county of Anhui province) is 1.27 million and the area covers 2968  $\text{km}^2$  which includes 1.19 million hectares of farmland and 0.24 million hectares of paddy fields. It is one of major grain-producing areas along the Huaihe River. The burning of crop residue in the field, as a means of disposal after harvesting at the end of May and in October and November, is a common practice in this region. Aerosol loading from this source is significant and will be discussed in section 3. In addition, Shouxian is only 11 km from Huainan City which is a major production center for coal and another source of local aerosol loading. The observation

site is located at the edge of a rural town with a population of ~120,000 and is largely surrounded by farmland.

## 3. Results and Discussion

### 3.1. Daily Variation of Aerosol Properties

[12] Time series of daily average aerosol data for some important AOS aerosol parameters are shown in Figure 1: total scattering coefficients at 450 nm, 550 nm, and 700 nm (Figure 1a); the Ångström exponents at three wavelength pairs (red line for 700–550 nm, green line for 700–450 nm, and blue line for 550–450 nm) (Figure 1b); hemispheric backscattering fractions and submicron scattering fractions at three wavelengths (Figures 1c and 1d); absorption coefficients and single scattering albedos at 550 nm (Figures 1e and 1f). Aerosols passing through a 10 micron diameter cutpoint impactor were measured. The gaps in the plots represent data either rejected during the quality assurance process or missing from the record due to instrument failure.

[13] The daily average data often showed considerable variability over relatively short time scales (e.g., 2–3 days). Aerosol particles tend to accumulate in the atmosphere for a few days, and then dissipate due to the passage of a cold front, dry deposition or a precipitation event. In addition, the large day-to-day variation of aerosol optical properties is driven by many meteorological variables, including air-parcel trajectory, level of stagnation, temperature inversion, and aerosol transport [Eck *et al.*, 2005; Z. Li *et al.*, 2007a].

[14] The plots of light scattering coefficients, hemispheric backscattering fractions, and submicron scattering fractions at three wavelengths are similar. Generally, the total scattering coefficients at 450 nm and 700 nm are about 130% and 75%, respectively, of the value at 550 nm. The submicron scattering ratios at 450 nm and 700 nm are about 109% and 90%, respectively, of the value at 550 nm. The hemispheric backscattering ratios increased with increasing wavelength due to decreasing size parameters. The mean values and standard deviations of  $\sigma_{sp}$ ,  $b$ , and  $R_{sp}$  at the green wavelength are  $401.2 \pm 314.3 \text{ Mm}^{-1}$ ,  $0.101 \pm 0.017$  and  $0.47 \pm 0.15$ , respectively. Values for  $b$  and  $R_{sp}$  are lower than those at inland sites in the United States [Sheridan *et al.*, 2001]. In addition,  $b$  is also lower than that ( $0.124 \pm 0.015$ ) observed at Backgarden, a rural site located in the Pearl River Delta (PRD), approximately 60 km northwest of the megacity Guangzhou in southeast China [Garland *et al.*, 2008].

[15] The absorption coefficients are higher in late May and the beginning of June, which is probably related to local agriculture residue burning after harvesting. The  $\omega_o$  ranges from 0.8 to 1.0 and the mean and standard deviation is  $0.92 \pm 0.03$ . This value is close to the  $\omega_o$  of smoke-dominated haze at the Southern Great Plains site in the United States [Ziomon and Lohmann, 2003]. In Figure 1, the light scattering coefficients are positively correlated with the light absorption coefficients. The correlation coefficient is 0.85. Light scattering and absorption coefficients are lower in the summer. This can be explained by frequent precipitation in the summer (favorable for aerosol cleaning) and relatively higher mixing heights (favorable for aerosol transport to upper levels).

[16] The Ångström exponent is an indicator of particle size. Dust and sea salt aerosols, which are dominated by super micron particles, generally have the Ångström exponents

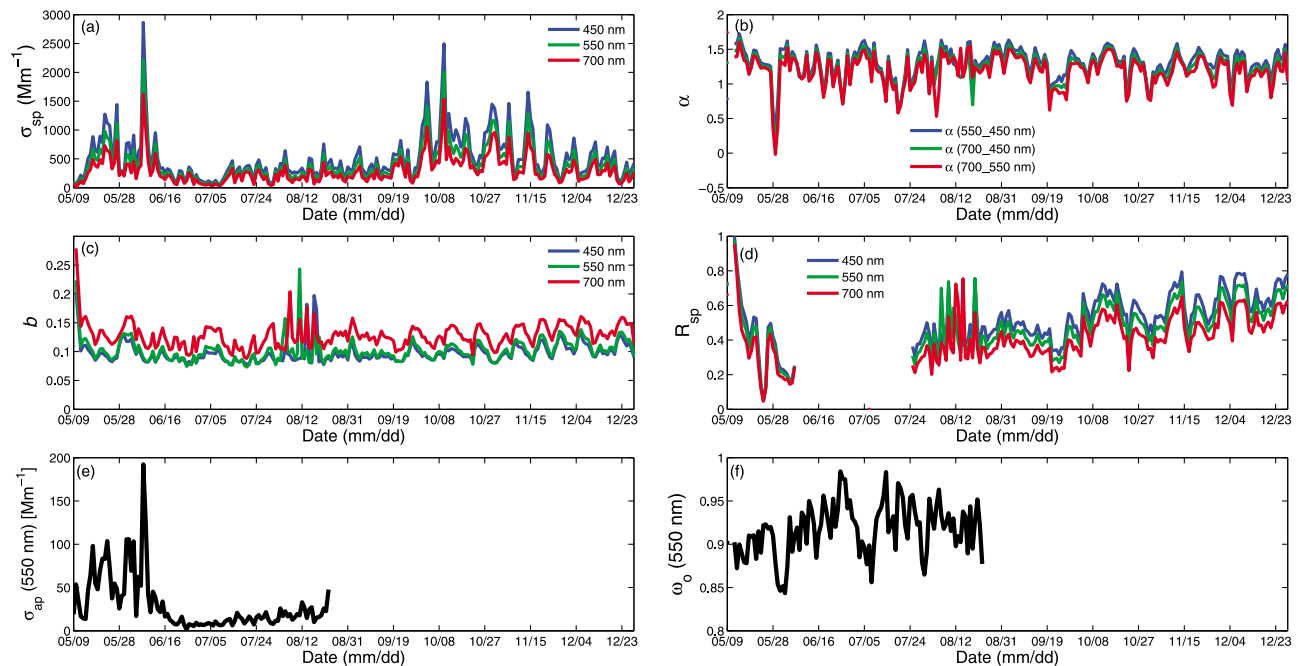


**Figure 1.** Eight month time series of daily average (a) total scattering coefficients at 450 nm, 550 nm, and 700 nm, (b) Ångström exponents at different wavelengths, (c) hemispheric backscattering coefficients at 450 nm, 550 nm, and 700 nm, (d) submicron scattering coefficients at 450 nm, 550 nm, and 700 nm, (e) absorption coefficients at 550 nm, and (f) single scattering albedos at 550 nm. The aerosols were passed through a 10 micron diameter cutpoint impactor.

close to zero. Pollution aerosols, the masses of which range from 0.1 to 1.0  $\mu\text{m}$ , usually have the Ångström exponents ranging from 2 to 3 [Peppler *et al.*, 2000]. Decreases in the Ångström exponent are thus indicative of a shift to coarse particles. As seen in Figure 1b, the exponents on 28, 29 and 30 May are 0.36,  $-0.002$ , and 0.37, respectively, which are much smaller than those on the other days. The extremely low Ångström exponents (including a negative value) suggest the transport of dust aerosols from northern China; this will be further discussed in section 3.3.2. Most Ångström exponents at Shouxian vary from 0.7 to 1.5, which accounts for 93% of observations. The 8 month averaged value of the Ångström exponent (700–550 nm) is  $1.19 \pm 0.23$ , which suggests a mixture of fine and coarse mode particles at Shouxian. The mean value of the Ångström exponent is close to that (1.17) at Taihu [Xia *et al.*, 2007], although the value at the Taihu site is derived from Sun photometer measurements representing the column value, while the values at Shouxian denote ground level. These values are significantly lower than those ( $1.51 \pm 0.22$ ) measured at Backgarden by the same instrument in a rural area near Guangzhou, China [Garland *et al.*, 2008]. The lower  $b$ ,  $R_{sp}$ , and Ångström exponents imply that particles at Shouxian are coarser than the other site.

[17] Table 2 summarizes the scattering and absorption coefficients and single scattering albedos observed in this study in comparison with those from other campaigns in different parts of China [Bergin *et al.*, 2001; Xu *et al.*, 2002, 2004; Yan, 2006; Pan, 2007; C. Li *et al.*, 2007; Andreae *et al.*, 2008; Cheng *et al.*, 2008; Garland *et al.*, 2008]. A brief introduction to the different sites listed in Table 2 is given

here. Beijing is the capital of China and a megacity with a population of 16 million; Peking University is located in the northwest part of Beijing. Both sites are influenced by urban aerosols. Shangdianzi is located in an outer suburb of Beijing where aerosol loading is considered to be at a background level. Xianghe is located about 70 km southeast of Beijing and is surrounded by agricultural land, densely occupied residences and light industry [C. Li *et al.*, 2007]; Baodi is another site located near Beijing which is characterized by rural aerosols. Yulin is located in northern Shanxi Province, close to the border with Inner Mongolia at the junction of the Gobi desert and the Loess Plateau [Xu *et al.*, 2004]. PRIDE-PRD campaigns were carried out in the Pearl River Delta (PRD) region, where the observation station at Guangzhou (the capital city of Guangdong Province) is located in an urban setting near major roads with a high traffic density; urban aerosols are typical for this area [Andreae *et al.*, 2008]. The Xinken site is located near the mouth of the Pearl River and situated on the northwest-southeast axis between Guangzhou and Hong Kong. The air pollution at Xinken is influenced by local sources such as biomass burning, cooking, and exhaust plumes from diesel ships [Cheng *et al.*, 2008]. Backgarden a small village in a rural farming environment situated on the edge of the highly populated PRD region. The Linan site is located in an agricultural region of the Yangtze delta in close proximity to large urban sources of anthropogenic pollutants (189 km west-southwest of Shanghai, with a population of  $\sim 12$  million; 40 km west of Hangzhou, with a population of 1.1 million) [Xu *et al.*, 2002].

**Table 2.** Aerosol Scattering Coefficients, Absorption Coefficients, and Single Scattering Albedo Values Observed in the Study and Reported by Other Campaigns in Different Parts of China<sup>a</sup>

Location	Observation Time	$\lambda$ (nm)	$\sigma_{sp}$ (Mm <sup>-1</sup> )	$\sigma_{ap}$ (Mm <sup>-1</sup> )	$\omega_0$	Citation
Beijing (Peking University, 39.99°N, 116.31°E)	11–16 Jun 1999	$\sigma_{sp} = 530, \sigma_{ap} = 565$	488 ± 370	83 ± 40	0.84 ± 0.08	Bergin <i>et al.</i> [2001]
Beijing (Urban, 39.93°N, 116.33°E)	18 Mar to 19 Apr 2006	$\sigma_{sp} = 525, \sigma_{ap} = 532$	278.0 ± 248.1	33.1 ± 29.2	0.87 ± 0.05	Pan [2007]
Shangdianzi (outer suburb of Beijing 40.64°N, 117.09°E)	Apr 2003 to Jan 2005	$\sigma_{sp} = 525, \sigma_{ap} = 532$	174.6 ± 189.1	17.5 ± 13.4	0.88 ± 0.05	Yan [2006]
Xianghe (70 km SE from Beijing, 39.75°N, 116.96°E)	Mar 2005	$\sigma_{sp} = 550, \sigma_{ap} = 550$	468 ± 472	65 ± 75	0.81–0.85	Li <i>et al.</i> [2007]
Baodi, Tianjin (Rural, 39.73°N, 117.28°E)	24 Apr to 16 May 2006	$\sigma_{sp} = 525, \sigma_{ap} = 532$	302.1 ± 171.8	62.2 ± 40.0	0.83 ± 0.06	Pan [2007]
ACE-Asia, Yulin (38.33°N, 109.72°E)	30 Mar to 1 May 2001	$\sigma_{sp} = 530, \sigma_{ap} = 565$	158 ± 193	6 ± 11	0.95 ± 0.05	Xu <i>et al.</i> [2004]
PRIDE-PRD2004 Guangzhou (23.13°N, 113.26°E)	4 Oct to 5 Nov 2004	$\sigma_{sp} = 530, \sigma_{ap} = 565$	463 ± 178	92 ± 62	0.84 ± 0.05	Andreae <i>et al.</i> [2008]
PRIDE-PRD2004 Xinken (22.6°N, 113.6°E)	4 Oct to 5 Nov 2004	$\sigma_{sp} = 550, \sigma_{ap} = 550$	333 ± 138	70 ± 42	0.83 ± 0.05	Cheng <i>et al.</i> [2008]
PRIDE-PRD2006 Backgarden (60 km NE from Guangzhou, 23.55°N, 113.07°E)	Jul 2006	$\sigma_{sp} = 550, \sigma_{ap} = 532$	151 ± 103	34.3 ± 26.5	0.82 ± 0.07	Garland <i>et al.</i> [2008]
Linan (Yangtze delta, 30.28°N, 119.75°E)	Nov 1999	$\sigma_{sp} = 530, \sigma_{ap} = 565$	353 ± 202	23 ± 14	0.93 ± 0.04	Xu <i>et al.</i> [2002]
Linan (Yangtze delta, 30.28°N, 119.75°E)	Jul 2003 to Jun 2005	$\sigma_{sp} = 525, \sigma_{ap} = 532$	242.1 ± 133.8	45.0 ± 22.1	0.82 ± 0.04	Yan [2006]
Shouxian (Eastern China, 32.56°N, 116.78°E)	May–Dec 2008	$\sigma_{sp} = 550, \sigma_{ap} = 550$	401.2 ± 314.3	29.4 ± 31.1	0.92 ± 0.03	This study

<sup>a</sup>Given as arithmetic mean ± std. dev.

[18] The measured  $\sigma_{ap}$  value at the Shouxian site is lower than most measurements made in urban areas in China; however, the  $\sigma_{ap}$  value is still higher than those observed in Yulin and in Shangdianzi. The measured  $\sigma_{sp}$  value at the Shouxian site is smaller than measurements made in Guangzhou, Xianghe and Beijing; however the  $\sigma_{sp}$  value is much higher than results from many other sites in China. The  $\omega_0$  value at the Shouxian site is higher than measurements made in PRD, the Yangtze Delta and northern China, indicating less absorbing aerosols at the Shouxian site.

### 3.2. Diurnal and Seasonal Variation of Aerosol Properties

[19] Hourly statistics of aerosol properties ( $D_p < 10 \mu\text{m}$ ) are represented as box-and-whiskers plots in Figure 2. In the plot, the ends of each box represent the 25th and 75th percentiles of the distribution, the ends of the whiskers represent the 5th and 95th percentiles, and the line across the box is the median of the distribution. The mean is represented by the diamond symbol. The horizontal line extending across all distributions is the median for all hourly data. Figures 2a, 2b, 2c, 2d, 2e, and 2f are the diurnal variations of scattering coefficients at 550 nm, Ångström exponents (700–550 nm), hemispheric backscattering fractions, submicron scattering fractions, absorption coefficients and single scattering albedos at 550 nm, respectively.

[20] The strongest diurnal variation is observed in absorption coefficients. The absorption coefficients are highest in the early morning, during the hours of 0500–0800 LT. There are relatively high local cooking emissions as well as emissions from transportation sources and agricultural machinery during this time period and there is very little atmospheric mixing. Median values start to decrease after 0800 LT and reach their lowest point during the hours of 1300–1600 LT. After 1700 LT, the median of the absorption coefficients begins to rise and remains elevated until 2200 LT; it then decreases again after 0800 LT in the following morning. This daily cycle is more pronounced when looking at the 75th and 95th percentile distributions. Light scattering coefficients show a similar daily cycle. Scattering coefficients also reach their lowest magnitude in the afternoon.

[21] The diurnal variability of temperature (T) and RH are shown in Figure 3. The daily minimum in T and maximum in RH occur around 0500 LT. The large difference between early morning and afternoon mean temperatures (7°C) suggests that the mixing height increases during the daytime. After sunrise, the temperature and therefore mixing height increase. This leads to the dilution of surface aerosols with air aloft and results in a corresponding decrease in  $\sigma_{sp}$  and  $\sigma_{ap}$  [Xu *et al.*, 2004]. The  $\sigma_{sp}$  and  $\sigma_{ap}$  begin to rise after sunset because the decrease in the surface temperature creates a temperature inversion and hence a stable atmospheric boundary layer. The presence of the temperature inversion minimizes the vertical mixing of aerosol particles. Aside from meteorological factors, stronger emissions during the morning/late afternoon rush hours may also enhance the peak pollutant levels. In addition, residential emissions are highest during breakfast and dinner hours among the rural households in China [Wang *et al.*, 2005]. The diurnal patterns of scattering and absorption coefficients were also observed at the Linan and Yulin site [Xu *et al.*, 2002].

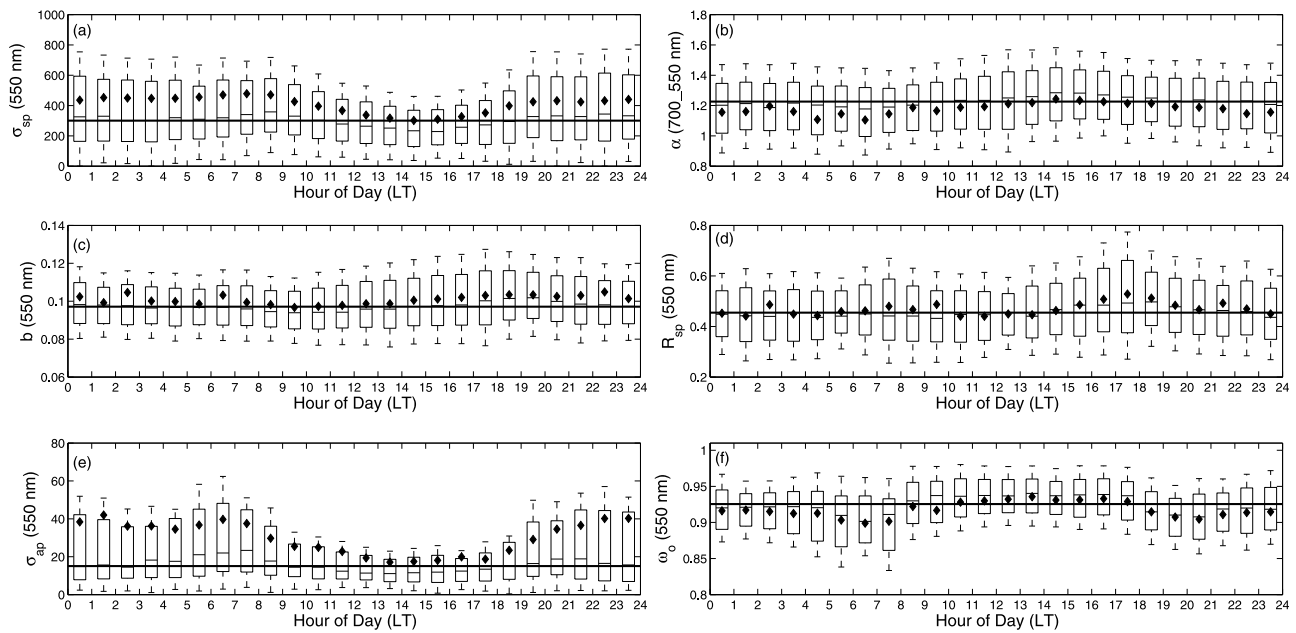


**Figure 2.** Statistical analysis showing hourly averaged aerosol properties for the 8 month period, sorted by hour of the day. The ends of the boxes, the ends of the whiskers, and the short line across each box represent the 25th and 75th percentiles, the 5th and 95th percentiles, and the median, respectively. The mean is represented by the diamond. The median line for that distribution is drawn across the entire plot. (a) Scattering coefficients at 550 nm, (b) Ångström exponents (700–550 nm), and (c) hemispheric back-scattering fractions, (d) submicron scattering fractions, (e) absorption coefficients, and (f) single scattering albedos at 550 nm.

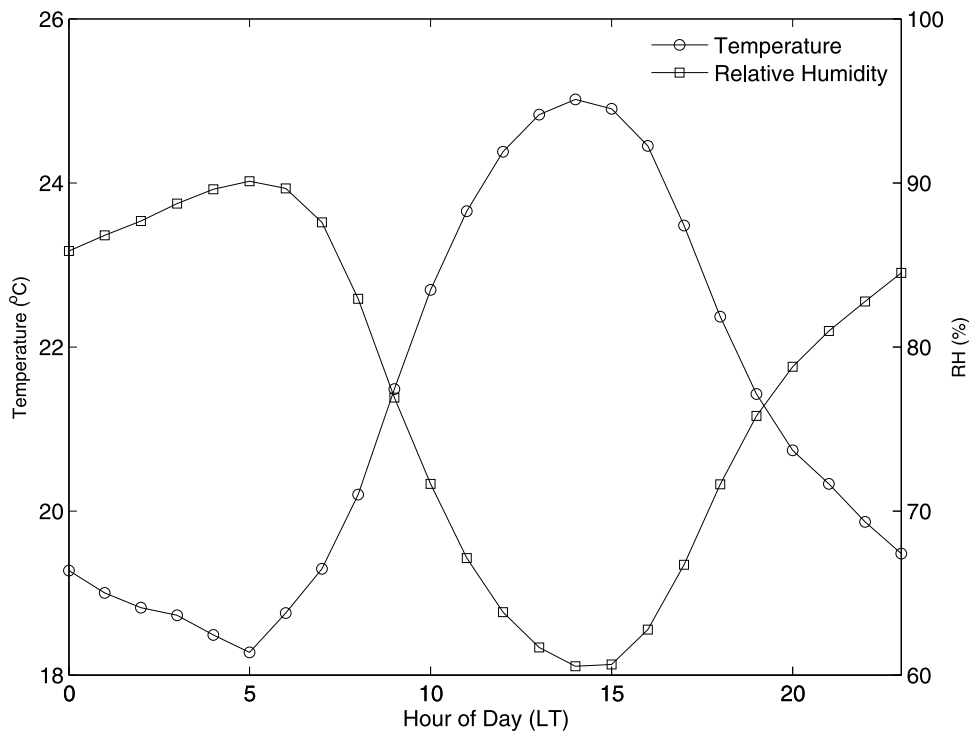


**Figure 3.** Time series of temperature (T) and relative humidity (RH). The values are averaged for each hour of the day during the 8 month observational period (9 May to 28 December 2008).

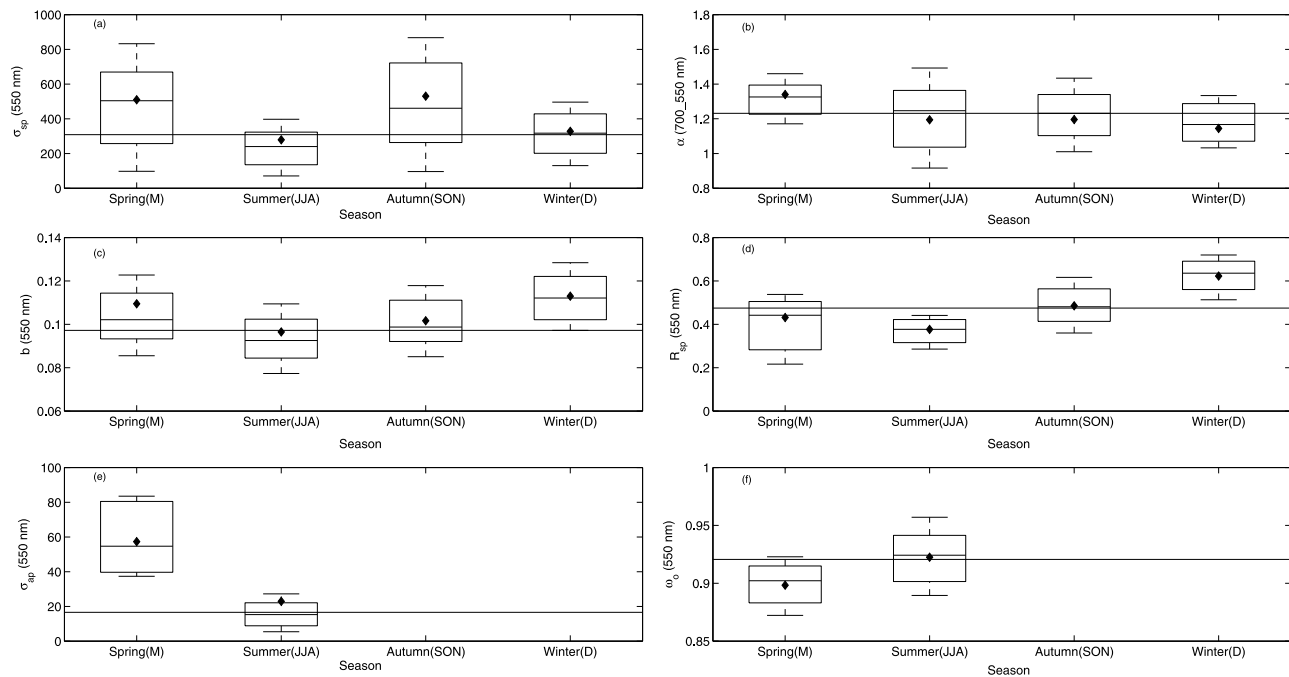


**Figure 4.** Same as Figure 2 but sorted by season: spring (May), summer (June, July, and August), autumn (September, October, and November), and winter (December).

[22] The single scattering albedo has nearly the same cycle as the absorption coefficient but with maximum and minimum values occurring during the afternoon and early morning, respectively. Maximum values occur near local noon, and the variability in the distribution is smaller near noon. This daily cycle was also observed at the Southern Great Plains site and the Bondville, Ill. surface monitoring site in the United States [Delene and Ogren, 2002]. The median value of  $\omega_o$  for the study period was about 0.92.

[23] Ångström exponents are lower at midnight and in the early morning (2200–0900 LT), which is possible due to aerosol hygroscopic growth from higher humidity. The median value of the Ångström exponent for the study period is about 1.23. The diurnal variation of hemispheric backscattering and submicron scattering fractions is similar to that of the Ångström exponent, because all three parameters depend on aerosol particle size.

[24] Figure 4 shows the seasonal distribution of hourly average aerosol properties. With the exception of  $\omega_o$ , all other parameters have their highest magnitude in the springtime due to the production of more fine-mode aerosols from agriculture residue burning at the end of May. Given that there are more absorbing aerosols then,  $\omega_o$  is low. The  $\sigma_{sp}$  and  $\sigma_{ap}$  are lower during the summer because there is more frequent precipitation and relatively higher mixing heights. Aerosol particles are bigger because of aerosol hygroscopic growth from higher RH in the summertime. So the Ångström exponent,  $b$  and  $R_{sp}$  are lower then. Autumn is the harvest season and the increase in aerosol production from agriculture residue burning is reflected in larger values of  $\sigma_{sp}$ ,  $\alpha$ ,  $b$  and  $R_{sp}$ .

### 3.3. Case Study

[25] As seen in Figures 1a and 1e, unusually high light scattering coefficients and absorption coefficients appear in

late May and at the beginning of June. There are also several peaks in light scattering coefficient in October and November. The elevated levels of aerosol light scattering and absorption coefficients strongly suggest an occurrence of significant pollution events. Two cases using satellite data together with ground measurements are described in this section. One case is a local agricultural burning pollution episode (22–23 May) and the other is a case influenced by a dust storm from northern China (28–30 May). Aerosol optical properties for the two cases including the median and mean values during the observation period are given in Table 3. Satellite observations and back trajectory analysis are further used to understand these cases. Satellite observations include MODIS fire products that provide the daily location of fire “hot spots” globally [Justice et al., 2002] and AOD retrievals [Remer et al., 2005; Levy et al., 2007]. The AOD is an important parameter reflecting aerosol optical properties and aerosol loading. The MODIS daily level 2 data are produced at the spatial resolution of a 10 by 10 km (at nadir) pixel array. In this study, we use daily AOD from the MODIS data set at 550 nm (<http://ladsweb.nascom.nasa.gov/data/>). Back trajectories provide valuable information on the origin of an air mass over the few days prior to its arrival at a particular site [Slingo et al., 2008]; this further aids in interpreting the AMF measurements at Shouxian. In this section, back trajectories are calculated using Version 4 of the HYSPLIT model (R. R. Draxler and G. D. Rolph, HYSPLIT Model, 2010, <http://ready.arl.noaa.gov/HYSPLIT.php>; G. D. Rolph, Real-time Environmental Applications and Display sYstem (READY), 2010, <http://ready.arl.noaa.gov>). The trajectory calculations use analyses from the National Centers for Environmental Prediction (NCEP) Global Data Assimilation System (GDAS). The output of the HYSPLIT4 model is hourly trajectory endpoints indicating the location (latitude and longitude) and height of the air parcel. Data collected

**Table 3.** Aerosol Optical Properties for the Two Pollution Cases, as Well as Mean and Median Values Over the 8 Month Campaign

Date	$\sigma_{sp}$ (550 nm) ( $Mm^{-1}$ )	$\sigma_{ap}$ (550 nm) ( $Mm^{-1}$ )	$\omega_0$ (550 nm)	$\alpha$ (700–550 nm)	$R_{sp}$ (550 nm)	b (550 nm)
22 May	980.1	82.9	0.91	1.30	0.30	0.099
23 May	866.1	103.6	0.89	1.23	0.14	0.096
28 May	223.5	25.7	0.91	0.36	0.42	0.112
29 May	273.6	40.3	0.88	-0.02	0.38	0.125
30 May	222.5	42.4	0.85	0.38	0.28	0.128
Median	302.8	16.7	0.92	1.23	0.47	0.098
Mean	401.2 $\pm$ 314.3	29.4 $\pm$ 31.1	0.92 $\pm$ 0.03	1.19 $\pm$ 0.23	0.47 $\pm$ 0.15	0.101 $\pm$ 0.017

by the MPL, an autonomous, eye-safe lidar system (532 nm) which operated continuously from 14 May to 28 December 2008 at the Shouxian site, is also used in the analysis. The cases presented below would help researchers to select ideal conditions to study the impact of different types of aerosols commonly encountered in China.

### 3.3.1. Agricultural Field Burning Event

[26] The period from the end of May to the beginning of June is the harvest season in central eastern China. Unregulated crop residue burning in the field is a common practice by some farmers which can result in serious local and regional environmental pollution. A study showed that Anhui is one of top three provinces in China with the most fire spots due to agriculture burning during the harvest season [Li *et al.*, 2009]. Figure 5 shows the variations of aerosol optical properties and meteorological factors including RH and wind vector during an agricultural burning pollution event from 19 to 25 May 2008. Time series of  $\omega_0$  (in red), light

scattering (in black) and absorption (in blue) coefficients are shown in Figure 5a. Figure 5b shows the time series of the Ångström exponent (in red), and hemispheric backscattering ratios (in blue). Note that light absorption coefficients ( $\sigma_{ap}$ ) and hemispheric backscattering ratios (Figure 5b) are multiplied by 10. The relative humidity during the same period is shown in Figure 5c and wind vectors are shown in Figure 5d. The light absorption coefficient on 22 May reaches  $82.9 Mm^{-1}$ , which is almost 5 and 3 times greater than the median and mean values, respectively, during the observation period. In Figure 5a, variations in  $\sigma_{sp}$  and  $\sigma_{ap}$  were similar except during the first half of 22 May. Both light scattering and absorption coefficients began to increase from the late night of 20 May and remained relatively high until 24 May. Scattering and absorption coefficients started to decrease from the afternoon of 24 May, when a change in wind shear from the southeast to the northeast occurred. This change in wind shear is favorable for aerosol dissipation. The

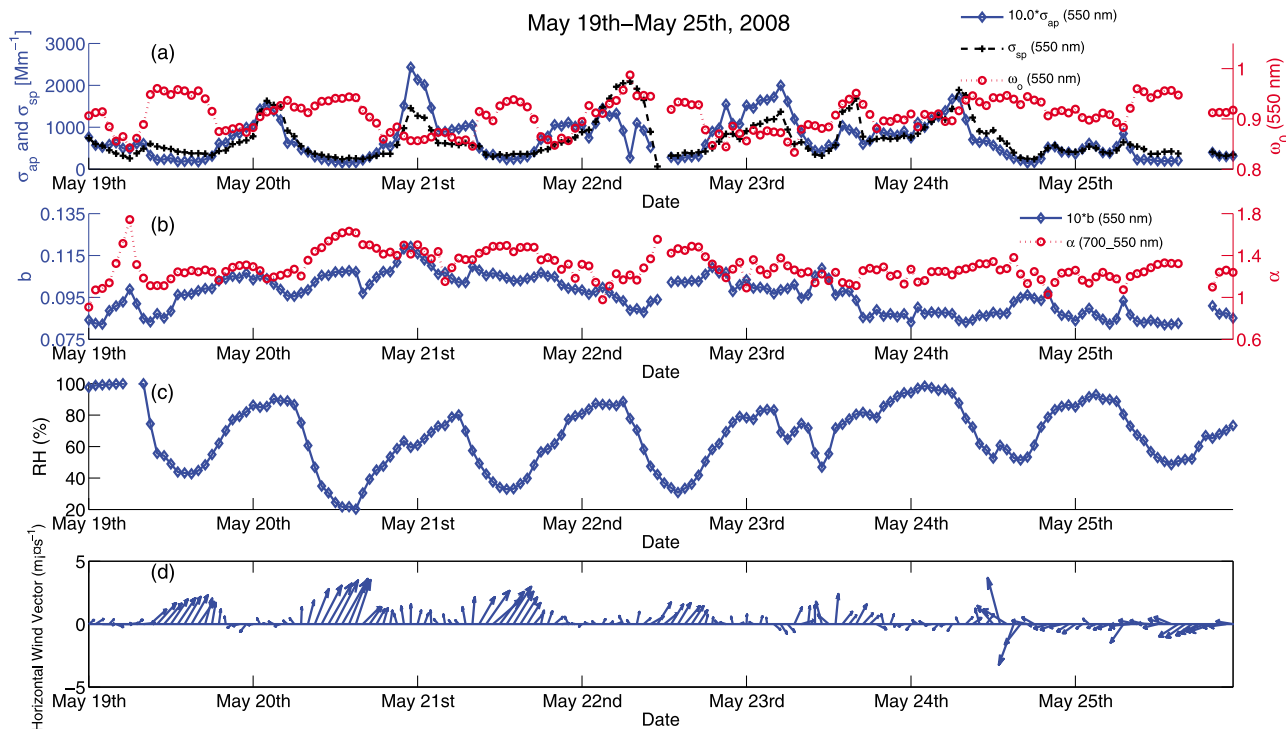


**Figure 5.** Time series of (a)  $\omega_0$  at 550 nm (red line), light scattering coefficient (black line), and absorption coefficient (blue line), (b) Ångström exponent (red line) and hemispheric backscattering fraction (blue line), (c) RH, and (d) horizontal wind vector. The time period is 19–25 May 2008. Note that for visual clarity, light absorption coefficients and hemispheric backscattering fractions are multiplied by 10.

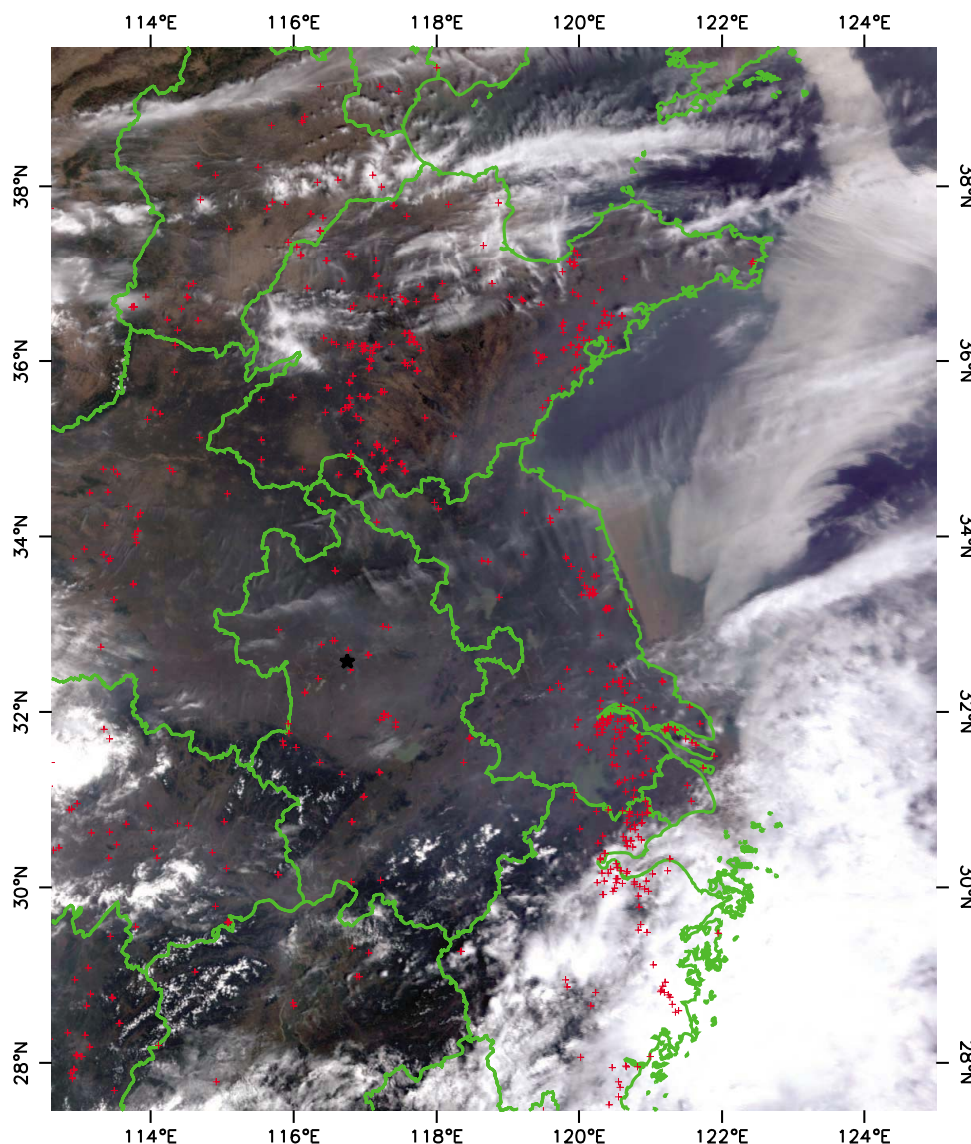


**Figure 6.** MODIS level 1B RGB composite image overlaid by the MODIS level 2 fire “hot spots” data (red pluses) over eastern China on 22 May 2008. The location of Shouxian is given by the black star.

absorption coefficient peaked at midnight on 21 May and  $\omega_0$  reached a minimum value of 0.85 at the same time. Light scattering and absorption coefficients are inversely correlated during the first half of 22 May. At 0800 LT on 22 May, there was a peak in the scattering coefficient and a trough in the absorption coefficient which resulted in a maximum value of  $\omega_0$  (0.99). The high RH and low wind speed during this time (Figures 5c and 5d) encourages stronger aerosol hygroscopic growth and accumulation. Variations in the Ångström exponent are similar to those of the hemispheric backscattering ratio as shown in Figure 5b. Both the Ångström exponents and hemispheric backscattering ratios show slightly higher values from 20–24 May, which indicates that there were more fine particles during this higher aerosol loading period.

[27] Figure 6 shows the MODIS level 1B RGB composite image overlaid by MODIS level 2 fire hot spots in eastern China on 22 May 2008. The black pentagram shows the

location of Shouxian. A widespread fire area is evident in the image. MODIS visible RGB imagery shows the areal extent of smoke and haze over Anhui, Jiangsu, Henan, and Shandong provinces. The fire area is in good agreement with the smoke area, which indicates that the aerosol loading in this case is mostly due to crop residue burning. MODIS/Terra level-2 AOD at 550 nm on 22 May are shown in Figure 7. Figure 7 is also overlaid with 3 day backward trajectories calculated for air arriving at Shouxian at heights of 500 m (red line), 1 km (blue line), and 4 km (black line) at 1200 LT (0400 UTC) on 22 May. The highest MODIS/Terra AOD (about 1.8) is over Anhui province where the Shouxian site is located. The high AOD region, which includes Henan, Jiangsu, Anhui and Shandong provinces, is consistent with the fire hot spot distribution shown in Figure 6. The backward trajectories illustrate air whirled over central China from the southwest where agriculture burning is evident from MODIS fire spot data. This indicates that the high

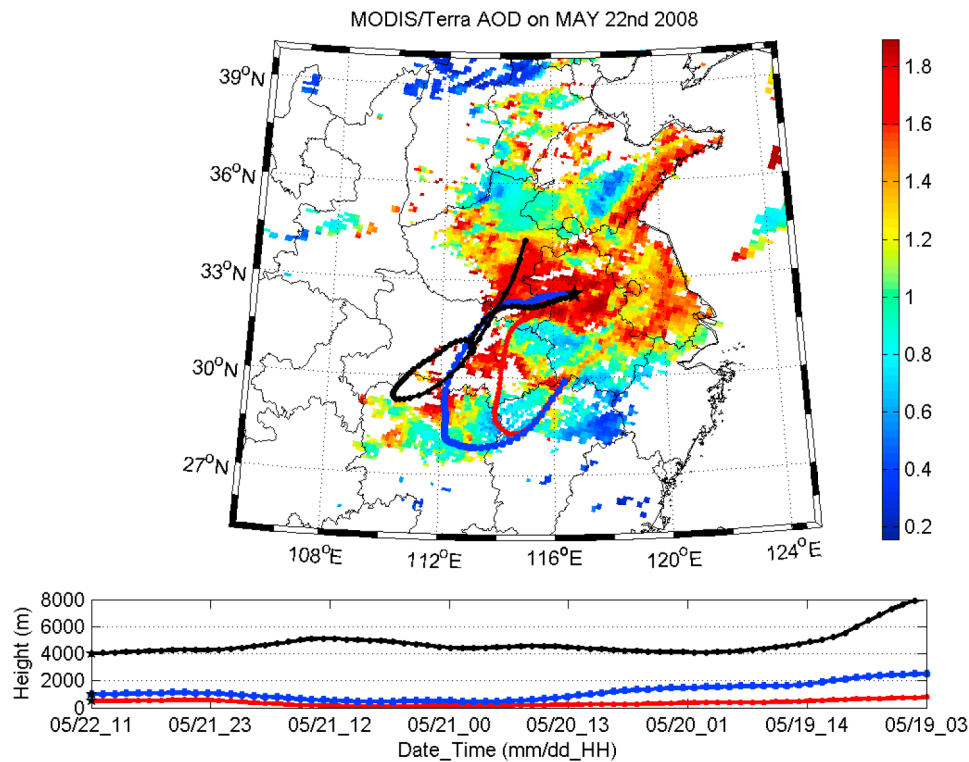


**Figure 7.** Spatial distribution of MODIS/Terra AOD overlaid by 3 day backward trajectories arriving at 1200 LT on 22 May 2008 (red line is at 500 m, blue line is at 1 km, and black line is at 4 km). The black star indicates the location of the Shouxian site.

aerosol loading during this case originated from local agricultural field burning rather than from distant sources.

### 3.3.2. Dust Event

[28] From 28 to 30 May, the Ångström exponents were extremely low and negative values appeared on 29 May (Figure 1b). Very low Ångström exponents indicate the presence of dust coarse particles. A large-scale dust event spread over northern China during the period of 26–28 May. The visibility in some regions of Inner Mongolia was less than 1 km. Prevalent northerly winds blew dust particles over the observation site at Shouxian. On 28 May, fine particles in the air, the main contributor to scattering, were dissipated by strong winds with speeds greater than  $7 \text{ m s}^{-1}$  which lead to low scattering and absorption coefficients. In addition, for coarse mode particles (diameters greater than  $1 \mu\text{m}$ ), nephelometer errors increase dramatically for total scattering (20–50%). The increase in error reflects the inability of a nephelometer to sense near forward scattering, which is an increasingly dominant part of total scattering for large particles [Anderson *et al.*, 1996]. Submicron scattering ratios were far less than the mean value. Low Ångström exponent and  $R_{sp}$  values suggest the dominant contribution from dust particles.

[29] MODIS/Aqua level-2 AODs at 550 nm on 28 May is shown in Figure 8, which is overlaid with 3 day backward trajectories calculated for air arriving at Shouxian at heights of 500 m (red line), 1 km (blue line), and 4 km (black line) at 1400 LT (0600 UTC) on 28 May. The highest MODIS/Aqua AOD (over 2.0) appeared over the Bohai Sea and along the coastal regions of the Yellow Sea in Shandong

province, which is consistent with the transported blanket of dust seen in the MODIS/Aqua level-1 RGB image (not shown here; see [http://modis-atmos.gsfc.nasa.gov/IMAGES/MYD02/GRANULE/2008\\_05\\_28/149.0550.rgb143.jpg](http://modis-atmos.gsfc.nasa.gov/IMAGES/MYD02/GRANULE/2008_05_28/149.0550.rgb143.jpg)). High AODs (over 1.0) were retrieved around the Shouxian site, where the MODIS/Aqua RGB image displayed floating dust. The dominant airflow into Shouxian was from the north and northwest at all levels, which implies that the high aerosol loading stem from long-distance dust transport. The extremely low Ångström exponents from AOS observations during this period corroborate the presence of dust aerosols over Shouxian.

[30] The MPL at Shouxian also observed the dust event around the site. Time series of attenuated backscatter profiles and linear depolarization ratios from 27 to 30 May are shown in Figure 9. For round particles, such as the stratospheric aerosols, the depolarization ratio is close to zero. For particles with unsymmetrical shapes, the depolarization ratio is nonzero. The depolarization ratios of dust aerosols have been found with values 0.2–0.5 in various researches [Cairo *et al.*, 1999]. In Figure 9, MPL signals were blocked by clouds during the daytime hours of 27 May. At about 0300 LT on 28 May, attenuated backscattering coefficients near the surface (0–2 km) began to increase and remained high until about 2200 LT. Strong winds with speeds greater than  $7 \text{ m s}^{-1}$  during the afternoon of 28 May favored the dissipation and dry deposition of dust particles. This reduced the magnitudes of the attenuated backscattering coefficients below the 1 km level. On 29 May, wind speeds decreased and backscattering coefficients increased again as aerosols began to accumulate. During this time, the linear

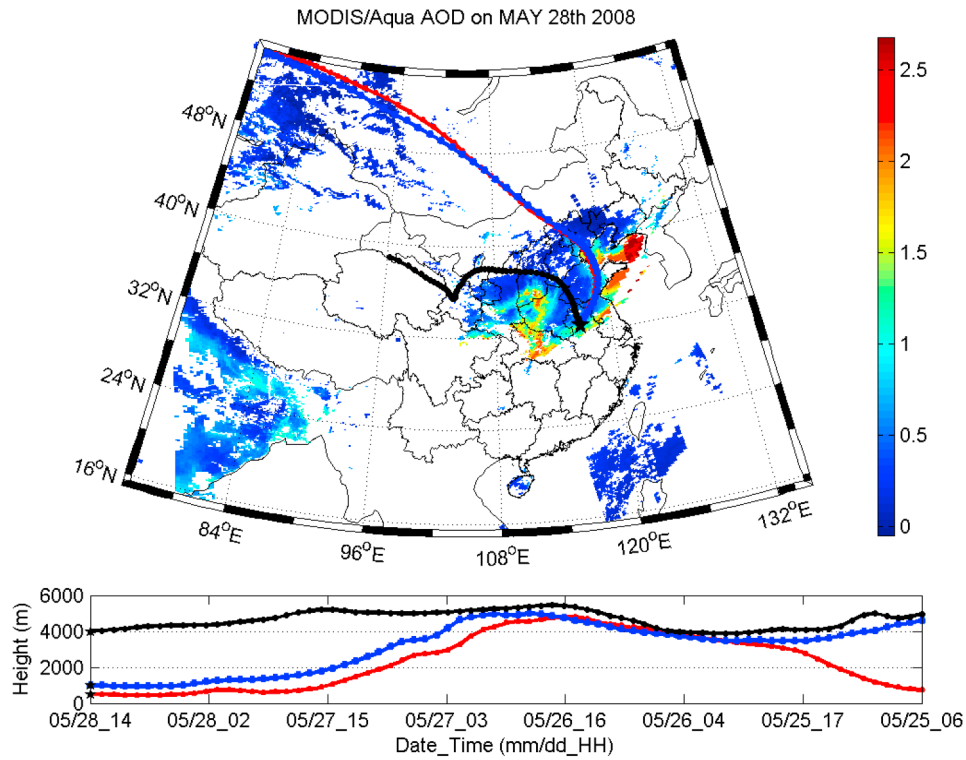


Figure 8. Same as Figure 7 but for MODIS/Aqua AOD and the backward trajectories arriving at 1400 LT on 28 May 2008.

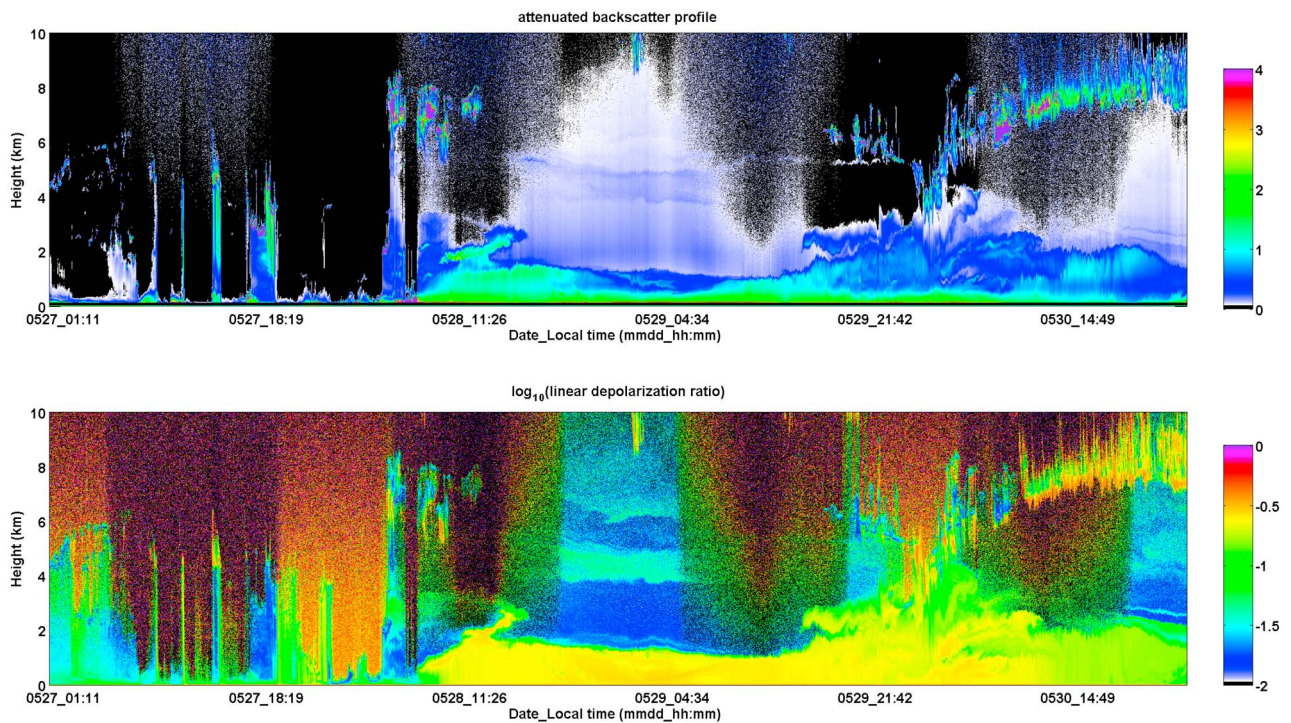


Figure 9. Time-height plots of (top) total lidar attenuated backscatter profiles and (bottom) linear depolarization ratio profiles for 27–30 May 2008.

depolarization ratio was constant with a high value of 0.2 (corresponding to a value of  $-0.7$  in Figure 9), which indicated that a dust aerosol layer was present around Shouxian.

#### 4. Summary

[31] Aerosol optical properties relevant to climate forcing were measured in eastern China during the 8 month deployment of the ARM's Mobile Facility (AMF) at Shouxian ( $32.56^{\circ}\text{N}$ ,  $116.78^{\circ}\text{E}$ ) in 2008. Analysis of the data collected by the AOS indicates that there is a complex mix of dust and smoke aerosols frequently present at the site.

[32] Averaged over the measurement campaign (arithmetic mean  $\pm$  standard deviation), the total scattering coefficients were  $518.3 \pm 402.2 \text{ Mm}^{-1}$  (450 nm),  $401.2 \pm 314.3 \text{ Mm}^{-1}$  (550 nm) and  $302.7 \pm 235.6 \text{ Mm}^{-1}$  (700 nm) and the absorption coefficient was  $29.4 \pm 31.1 \text{ Mm}^{-1}$  (550 nm). The averaged single scattering albedo was  $0.92 \pm 0.03$  (550 nm), which is higher than that found from measurements made in the Pearl River Delta, the Yangtze Delta and northern China, indicating less absorbing aerosols at the Shouxian site.

[33] The averaged Ångström exponent was  $1.19 \pm 0.23$  (700–550 nm), which is lower than that found in the Pearl River Delta region of China. The mean values and standard deviations of submicron scattering ratios and hemispheric backscattering ratios at 550 nm were  $0.47 \pm 0.15$  and  $0.101 \pm 0.017$ , respectively, which is lower than values found at several inland sites in the United States. This implies that the contribution of local floating dust and soot due to human activities is significant.

[34] The strongest diurnal variation is observed in absorption coefficients. The absorption coefficients are highest in the early morning with minimum values occurring at noon. The diurnal variation of  $\omega_o$  was similar to that of the absorption coefficient except that the maximum and minimum values occurred around noon and in the early morning, respectively. The magnitudes of the Ångström exponent were lowest at midnight and during the early morning hours. This is likely due to aerosol hygroscopic growth from higher humidity.

[35] In addition, MPL data, back trajectories and MODIS aerosol and fire products were combined to investigate periods when the ambient aerosols were significantly impacted by dust and smoke.

[36] These surface aerosol measurements obtained during the 8 month deployment at Shouxian in eastern China, especially the heavy smoke and dust cases identified, will help validate satellite retrievals, understand the mechanisms of aerosol climatic effects in the region, and examine the roles which aerosols may play in regional climate and atmospheric circulation, with a special focus on the impact of the East Asian monsoon system.

[37] **Acknowledgments.** The work was mainly supported by National Basic Research Program of China under grant 2010CB950804, the National Science Foundation of China (grant 40805010), the Knowledge Innovation Program of the Chinese Academy of Sciences (grant KZCX2-YW-QN201), Key Projects in the National Science and Technology Pillar Program in the Eleventh Five-Year Plan Period (2008BAC40B01), the DOE/ARM (DEFG0208ER64571-S01), NASA (NNX08AH71G), and MOST (2006CB403706). The authors gratefully acknowledge the NOAA Air Resources Laboratory (ARL) for the provision of the HYSPLIT transport and dispersion model and/or READY Web site (<http://www.arl.noaa.gov/>

ready.php) used in this publication. We also thank Minnie Wong from the Geography Department, UMD, for providing MODIS fire products and Liang Peng for his help in plotting.

#### References

- Anderson, T. L., et al. (1996), Performance characteristic of a high-sensitivity, three-wavelength, total scatter/backscatter nephelometer, *J. Atmos. Oceanic Technol.*, *13*, 967–986, doi:10.1175/1520-0426(1996)013<0967:PCOAHS>2.0.CO;2.
- Andreae, M. O., O. Schmid, H. Yang, J. Z. Yu, and Y. H. Zhang (2008), Optical properties and chemical composition of the atmospheric aerosol in urban Guangzhou, China, *Atmos. Environ.*, *42*, 6335–6350, doi:10.1016/j.atmosenv.2008.01.030.
- Bao, Z. H., Z. P. Wen, and R. G. Wu (2009), Variability of aerosol optical depth over East Asia and its possible Impacts, *J. Geophys. Res.*, *114*, D05203, doi:10.1029/2008JD010603.
- Bergin, M. H., et al. (2001), Aerosol radiative, physical, and chemical properties in Beijing during June 1999, *J. Geophys. Res.*, *106*(D16), 17,969–17,980, doi:10.1029/2001JD900073.
- Bond, T. C., T. L. Anderson, and D. Campbell (1999), Calibration and inter-comparison of filter-based measurements of visible light absorption by aerosols, *Aerosol Sci. Technol.*, *30*, 582–600, doi:10.1080/027868299304435.
- Cairo, F., G. D. Donfrancesco, A. Adriani, L. Pulvirenti, and F. Fierli (1999), Comparison of various linear depolarization parameters measured by lidar, *Appl. Opt.*, *38*, 4425–4432, doi:10.1364/AO.38.004425.
- Che, H. Z., G. Y. Shi, X. Y. Zhang, R. Arimoto, J. Q. Zhao, L. Xu, B. Wang, and Z. H. Chen (2005), Analysis of 40 years of solar radiation data from China, 1961–2000, *Geophys. Res. Lett.*, *32*, L06803, doi:10.1029/2004GL022322.
- Che, H. Z., Z. Yang, X. Zhang, C. Zhu, Q. Mac, H. Zhou, and P. Wang (2009), Study on the aerosol optical properties and their relationship with aerosol chemical compositions over three regional background stations in China, *Atmos. Environ.*, *43*, 1093–1099, doi:10.1016/j.atmosenv.2008.11.010.
- Chen, R., H. Jiang, Z. Y. Xiao, S. Q. Yu, J. Li, and S. M. Hong (2008), Monitoring aerosol optical properties using ground based remote sensing and the change of atmospheric environment in Hangzhou region (in Chinese with English abstract), *Res. Environ. Sci.*, *21*(3), 22–26.
- Cheng, Y. F., et al. (2008), Aerosol optical properties and related chemical apportionment at Xinken in Pearl River Delta of China, *Atmos. Environ.*, *42*, 6351–6372, doi:10.1016/j.atmosenv.2008.02.034.
- Delene, D. J., and J. A. Ogren (2002), Variability of aerosol optical properties at four North American surface monitoring sites, *J. Atmos. Sci.*, *59*, 1135–1150, doi:10.1175/1520-0469(2002)059<1135:VOAOPA>2.0.CO;2.
- Eck, T. F., et al. (2005), Columnar aerosol optical properties at AERONET sites in central eastern Asia and aerosol transport to the tropical mid-Pacific, *J. Geophys. Res.*, *110*, D06202, doi:10.1029/2004JD005274.
- Garland, R. M., et al. (2008), Aerosol optical properties in a rural environment near the mega-city Guangzhou, China: Implications for regional air pollution, radiative forcing and remote sensing, *Atmos. Chem. Phys.*, *8*, 5161–5186, doi:10.5194/acp-8-5161-2008.
- Iziomon, M. G., and U. Lohmann (2003), Optical and meteorological properties of smoke-dominated haze at the ARM Southern Great Plains Central Facility, *Geophys. Res. Lett.*, *30*(3), 1123, doi:10.1029/2002GL016606.
- Jin, M. L., and J. M. Shepherd (2008), Aerosol relationships to warm season clouds and rainfall at monthly scales over east China: Urban land versus ocean, *J. Geophys. Res.*, *113*, D24S90, doi:10.1029/2008JD010276.
- Justice, C. O., L. Giglio, S. Korontzi, J. Owens, J. T. Morisette, D. Roy, J. Desclotres, S. Alleaume, F. Petitcolin, and Y. Kaufman (2002), The MODIS fire products, *Remote Sens. Environ.*, *83*, 244–262, doi:10.1016/S0034-4257(02)00076-7.
- Levy, R. C., L. A. Remer, and O. Dubovik (2007), Global aerosol optical properties and application to Moderate Resolution Imaging Spectroradiometer aerosol retrieval over land, *J. Geophys. Res.*, *112*, D13210, doi:10.1029/2006JD007815.
- Li, C. C., J. T. Mao, L. K. Alexis, J. C. Chen, Z. B. Yuan, X. Y. Liu, A. H. Zhu, and G. Q. Liu (2003), Characteristics of distribution and seasonal variation of aerosol optical depth in eastern China with MODIS products, *Chin. Sci. Bull.*, *48*(22), 2488–2495.
- Li, C., L. T. Marufu, R. R. Dickerson, Z. Q. Li, T. X. Wen, Y. S. Wang, P. C. Wang, H. B. Chen, and J. W. Stehr (2007), In situ measurements of trace gases and aerosol optical properties at a rural site in northern China during East Asian Study of Tropospheric Aerosols: An international regional experiment 2005, *J. Geophys. Res.*, *112*, D22S04, doi:10.1029/2006JD007592.
- Li, Q., L. J. Zhang, C. Q. Wu, Z. P. Sun, and X. M. Liu (2009), Satellite-remote-sensing-based monitoring of straw burning and analysis of its

- impact on air quality (in Chinese with English abstract), *J. Ecol. Rural Environ.*, 25(1), 32–37.
- Li, X. W., and X. J. Zhou (1995), The cooling of Sichuan province in recent 40 years and its probable mechanism, *Acta Meteorol. Sin.*, 9, 57–68.
- Li, Z., et al. (2007a), Preface to special section on East Asian Studies of Tropospheric Aerosols: An International Regional Experiment (EAST-AIRE), *J. Geophys. Res.*, 112, D22S00, doi:10.1029/2007JD008853.
- Li, Z., et al. (2007b), Aerosol optical properties and their radiative effects in northern China, *J. Geophys. Res.*, 112, D22S01, doi:10.1029/2006JD007382.
- Li, Z., K. H. Lee, Y. Wang, J. Xin, and W. M. Hao (2010), First observation-based estimates of cloud-free aerosol radiative forcing across China, *J. Geophys. Res.*, 115, D00K18, doi:10.1029/2009JD013306.
- Liang, F., and X. Xia (2005), Long-term trends in solar radiation and the associated climatic factors over China for 1961–2000, *Ann. Geophys.*, 23, 2425–2432, doi:10.5194/angeo-23-2425-2005.
- Luo, Y., D. Lu, X. Zhou, W. Li, and Q. He (2001), Characteristics of the spatial distribution and yearly variation of aerosol optical depth over China in last 30 years, *J. Geophys. Res.*, 106(D13), 14,501–14,513, doi:10.1029/2001JD900030.
- Pan, L., H. Che, F. Geng, X. Xia, Y. Wang, C. Zhu, M. Chen, W. Gao, and J. Guo (2010), Aerosol optical properties based on ground measurements over the Chinese Yangtze Delta Region, *Atmos. Environ.*, 44, 2587–2596, doi:10.1016/j.atmosenv.2010.04.013.
- Pan, X. L. (2007), Observation study of atmospheric aerosol scattering characteristics as a function of relative humidity (in Chinese with English abstract), Ph.D. thesis, Chin. Acad. of Meteorol. Sci., Beijing.
- Peppler, R. A., et al. (2000), ARM Southern Great Plains site observations of the smoke pall associated with the 1998 Central American fires, *Bull. Am. Meteorol. Soc.*, 81(11), 2563–2592, doi:10.1175/1520-0477(2000)081<2563:ASGPSO>2.3.CO;2.
- Qian, Y., D. P. Kaiser, L. R. Leung, and M. Xu (2006), More frequent cloud-free sky and less surface solar radiation in China from 1955 to 2000, *Geophys. Res. Lett.*, 33, L01812, doi:10.1029/2005GL024586.
- Remer, L. A., et al. (2005), The MODIS aerosol algorithm, products and validation, *J. Atmos. Sci.*, 62, 947–973.
- Sheridan, P. J., D. J. Delene, and J. A. Ogren (2001), Four years of continuous surface aerosol measurements from Department of Energy's Atmospheric Radiation Measurement Program Southern Great Plains Cloud and Radiation Testbed site, *J. Geophys. Res.*, 106(D18), 20,735–20,747, doi:10.1029/2001JD000785.
- Slingo, A., et al. (2008), Overview of observations from the RADAGAST experiment in Niamey, Niger: Meteorology and thermodynamic variables, *J. Geophys. Res.*, 113, D00E01, doi:10.1029/2008JD009909.
- Song, L., and D. R. Lu (2006), Investigation of atmospheric optical characteristics over Shanghai region (in Chinese with English abstract), *Clim. Environ. Res.*, 11(2), 203–208.
- Wang, X., D. L. Mauzerall, Y. Hu, A. G. Russell, E. D. Larson, J.-H. Woo, D. G. Streets, and A. Guenther (2005), A high-resolution emission inventory for eastern China in 2000 and three scenarios for 2020, *Atmos. Environ.*, 39, 5917–5933, doi:10.1016/j.atmosenv.2005.06.051.
- Xia, X. A., Z. Q. Li, B. Holben, P. C. Wang, T. Eck, H. B. Chen, M. Cribb, and Y. X. Zhao (2007), Aerosol optical properties and radiative effects in the Yangtze Delta region of China, *J. Geophys. Res.*, 112, D22S12, doi:10.1029/2007JD008859.
- Xin, J., et al. (2007), AOD and Angstrom exponent of aerosols observed by the Chinese Sun Hazemeter Network from August 2004 to September 2005, *J. Geophys. Res.*, 112, D05203, doi:10.1029/2006JD007075.
- Xu, J., M. H. Bergin, X. Yu, G. Liu, J. Zhao, C. M. Carrico, and K. Baumann (2002), Measurement of aerosol chemical, physical and radiative properties in the Yangtze delta region of China, *Atmos. Environ.*, 36, 161–173, doi:10.1016/S1352-2310(01)00455-1.
- Xu, J., M. H. Bergin, R. Greenwald, J. J. Schauer, M. M. Shafer, J. L. Jaffrezo, and G. Aymoz (2004), Aerosol chemical, physical, and radiative characteristics near a desert source region of northwest China during ACE-Asia, *J. Geophys. Res.*, 109, D19S03, doi:10.1029/2003JD004239.
- Xu, Q. (2001), Abrupt change of the midsummer climate in central east China by the influence of atmospheric pollution, *Atmos. Environ.*, 35, 5029–5040, doi:10.1016/S1352-2310(01)00315-6.
- Yan, P. (2006), Study on the aerosol optical properties in the background regions in the east part of China (in Chinese with English abstract), Ph.D. thesis, Peking Univ., Beijing.
- Yu, S., V. K. Saxena, and Z. Zhao (2001), A comparison of signals of regional aerosol-induced forcing in eastern China and the southeastern United States, *Geophys. Res. Lett.*, 28(4), 713–716, doi:10.1029/2000GL011834.
- Zhao, C., X. Tie, and Y. Lin (2006), A possible positive feedback of reduction of precipitation and increase in aerosols over eastern central China, *Geophys. Res. Lett.*, 33, L11814, doi:10.1029/2006GL025959.

H. Chen, X. Fan, and X. Xia, Key Laboratory of Middle Atmosphere and Global Environment Observation, Institute of Atmospheric Physics, Chinese Academy of Sciences, Beijing 100029, China. (fxh@mail.iap.ac.cn)  
M. Cribb and Z. Li, Department of Atmospheric and Oceanic Sciences, University of Maryland, College Park, MD 20740, USA.